Influence of walkoff on pattern formation in nondegenerate optical parametric oscillators

H. Ward,[1] M. N. Ouarzazi,[2] M. Taki,[1] and P. Glorieux[1]

[1]*Laboratoire de Physique des Lasers, Atomes et Molécules, CNRS UMR No. 8523, Centre d'Études et de Recherches Lasers et Applications, Université des Sciences et Technologies de Lille, UFR de Physique, Bâtiment P5, F-59655 Villeneuve d'Ascq Cedex, France*

[2]*Laboratoire de Mécanique de Lille, CNRS URA No. 1441, Université des Sciences et Technologies de Lille, F-59655 Villeneuve d'Ascq Cedex, France*

(Received 25 July 2000; published 19 December 2000)

Convective and absolute nature of instabilities in nondegenerate optical parametric oscillators with large transverse section, for negative detunings and in the presence of walkoff, is examined. The asymptotic response of the signal and idler fields to a transverse localized two-dimensional perturbation is evaluated. The presence of walkoff breaks the rotational symmetry in the transverse plane, and the system, at the absolute instability threshold, selects traveling waves propagating in the walkoff direction among an infinity of unstable spatiotemporal modes. We show that in optical parametric oscillators (OPO's) with negative detunings, contrary to the case of positive detunings, the walkoff shrinks the region of convective instabilities, and even may suppress the convective/absolute transition. Hence, in a certain range of parameters, signal field envelopes in the form of wave packets of zero group velocity are found where the instability is absolute at the onset, although the walkoff is present. We also show that nonlinear pattern selection is ruled by the cross-coupling terms appearing in the asymmetric coupled Ginzburg-Landau equations derived near-threshold of the signal and idler generation. The numerical solutions of the original OPO equations confirm the analytical predictions for the values of the instability thresholds and the corresponding selected patterns.

DOI: 10.1103/PhysRevE.63.016604 PACS number(s): 42.65.Yj, 47.54.+r, 42.60.Jf

I. INTRODUCTION

Pattern formation in extended systems has received a lot of attention in fields as different as physics, hydrodynamics, chemistry, and biology. The development of such studies is supported by the progress of theoretical methods and is motivated by practical situations in which this question arises. As far as optics is concerned, progress in the knowledge of pattern-formation mechanisms appears to be necessary to understand the behavior of large-area coherent sources such as vertical cavity semiconductor lasers or high-power optical oscillators. The transverse structure of the beam emitted by these oscillators is a key factor for their practical use. The structure must be mastered for applications including laser ranging, laser-induced fusion, or optical coherent information processing.

Transverse patterns in nonlinear optical systems have been widely studied since the early days of lasers. In the first approaches, a modal decomposition was sufficient to understand the experimental observations. By this technique, the laser field is projected on the basis provided by the empty cavity modes. These are Hermite-Gauss or Laguerre-Gauss modes for open cavities, depending on their symmetry, and guided modes for waveguide and fiber lasers. When the transverse section of the laser beams increases, this decomposition requires larger and larger basis sets, and it becomes inadequate for systems with large (about 100) Fresnel numbers.

In the global approach used for systems with a large Fresnel number, the partial differential equations describing the dynamics in the presence of diffraction have to be solved. Lasers belong to a family of nonlinear continuous systems where dissipative structures branch out of a homogeneous basic state when the external parameter exceeds a critical threshold. The distinction between absolute and convective instabilities in the unstable region is important to elucidate the mechanisms underlying the formation of these dissipative structures, and, in particular, to separate noise-sustained patterns from those originating from the intrinsic dynamics of the system. In the convectively unstable region, localized perturbations grow in a comoving frame, but are drifted out of the system in the absence of a continuous source of noise. In the absolutely unstable region, however, such perturbations grow with time at any spatial position, and therefore affect the system everywhere. In order to characterize the nature of the instability in various different physical systems, we give a unified description based on a classification of patterns in terms of the group velocity U^c of the most unstable mode. Class I_A systems are those characterized by the vanishing of U^c. Consequently, the basic state of these systems becomes directly absolutely unstable. Examples of class I_A systems are, in optics, optical parametric oscillators (OPO's) (respectively lasers) with positive (respectively negative) detuning [1,2], degenerate OPO's for both signs of detuning [3]; and in hydrodynamics, the well-known Rayleigh-Bénard convection, and Taylor vortex flow. Class I_C systems are those characterized by $U^c \neq 0$. These systems exhibit a region of convective instability. Examples of class I_C systems are OPO's (respectively lasers) with negative (respectively positive) detuning, and binary fluid mixture [4]. In these latter three examples, the system undergoes a Hopf bifurcation to symmetry degenerate left and right traveling wave patterns.

The question we want to approach now is the influence of an additional effect which breaks the reflection symmetry ($x \leftrightarrow -x$) in the transverse plane supposed present in both systems classified as I_A and I_C. Specifically, the knowledge of how this broken symmetry alters the convective/absolute

nature of the instability in both systems is necessary. The influence of this additional effect on the spatiotemporal behavior of class I_A systems has been the subject of extensive investigations in recent years: namely, the effect of walkoff in degenerate OPO's [5–10] and in nondegenerate OPO's without diffraction [11] and including diffraction [12]. This optical situation is analogous to that encountered in Rayleigh-Bénard convection and Taylor vortex flow where an externally imposed cross flow, is added in both systems [13]. In OPO's (respectively hydrodynamics), these studies reveal notably that the walkoff (respectively the imposed through-flow) creates necessarily a region of convective instability. Therefore, the nature of the instability changes from absolute to convective at the onset. These systems may also experience a second transition to absolute instability beyond the onset. We are not aware of similarly extensive studies of the influence of this broken symmetry phenomenon on pattern selection in class I_C systems. Let us cite two references dealing with binary fluid convection with added through-flow in fluid media [14], as well as in porous media [15].

In this paper, we concentrate on OPO's in the case of negative detuning which belongs to class I_C systems. The influence of walkoff is investigated and reveals new qualitative behaviors that are absent in our previous work [12] dealing with OPO's with positive detuning. The paper is organized as follows. In Sec. II, we recall the OPO governing equations, including walkoff and diffraction effects. Linear stability analysis of these equations is performed as an initial-value problem to obtain both the pump thresholds for the onset of convective and absolute instabilities, and the response of the system to two-dimensional (2D) localized perturbations. The convective instability criterion allows us to obtain the modulus of wave number at criticality, but there is still a spatial degeneracy due to all possible orientations of the wave vector. However, the linear absolute instability criterion shows that in most cases, the OPO selects a monodimensional structure in the walkoff direction, as was observed experimentally [16,17], but there remains a degeneracy between the positive and the negative directions. The possible transition to mixed mode patterns is then considered. Taking advantage of the 1D pattern-selection mechanism which exists in OPO's in the presence of walkoff, this is achieved by performing analytical studies on the corresponding amplitude equations. Section III deals with this approach to investigate the evolution of wave packets in the unstable region. The characteristics of the instabilities such as the thresholds and critical wave numbers and frequencies are analytically obtained with special emphasis on the case of small walkoff, valid in almost all experimental situations.

Numerical simulations of the full 2D OPO model are carried out to check the validity range of the analytical studies. They are reported in Sec. IV. Concluding remarks are summarized in the final section.

II. CONVECTIVE VERSUS ABSOLUTE INSTABILITIES IN OPO'S

A. Model

We start from the standard description [12] of an OPO in the mean-field approximation. It includes, in addition to the transverse Laplacian terms ($\nabla_\perp^2$) accounting for diffraction, drift terms (∂_x) describing walkoff effects:

$$\partial_t A_p = \gamma_p[-(1+i\Delta_p)A_p + E(x,y) - A_s A_i + i a_p \nabla_\perp^2 A_p],$$

$$\partial_t A_s = \gamma_s[-(1+i\Delta_s)A_s + A_p A_i^* + i a_s \nabla_\perp^2 A_s - \alpha_s \partial_x A_s], \quad (1)$$

$$\partial_t A_i = \gamma_i[-(1+i\Delta_i)A_i + A_p A_s^* + i a_i \nabla_\perp^2 A_i - \alpha_i \partial_x A_i],$$

where A_j with $j=p$, s, or i are the normalized slowly varying envelopes for pump, signal, and idler fields, respectively. The parameters Δ_j, γ_j, and a_j are the detunings, the cavity decay rates, and the diffraction coefficients, respectively. E is the normalized external pump and $\alpha_{s,i}$ are the signal and idler walkoff coefficients, respectively. Note that the above governing equations account for a type-I as well as a type-II OPO. For instance, type-II OPO's considered in [9] are obtained from Eqs. (1) by setting $\alpha_i = 0$ and keeping α_s, the polarization of the idler being, as the pump, ordinary, and the signal extraordinary [9,12]. Equations (1) have a homogeneous trivial time-independent (OPO OFF) solution:

$$A_p = E/(1+i\Delta_p) = \mu, \quad A_s = 0, \; A_i = 0, \quad (2)$$

and, a nontrivial one which exists only above threshold ($\mu > 1$).

It is convenient to rewrite Eqs. (1) in terms of the deviations from the equilibrium $B = A_p - \mu$, A_s, A_i which obey the following system:

$$\partial_t B = \gamma_p[-(1+i\Delta_p)B + i a_p \nabla_\perp^2 B - A_s A_i],$$

$$\partial_t A_s = \gamma_s[-(1+i\Delta_s)A_s + \mu A_i^* + i a_s \nabla_\perp^2 A_s - \alpha_s \partial_x A_s + A_i^* B], \quad (3)$$

$$\partial_t A_i^* = \gamma_i[-(1-i\Delta_i)A_i^* + \mu A_s - i a_i \nabla_\perp^2 A_i^* - \alpha_i \partial_x A_i^* + A_s B^*].$$

B. Linear stability analysis, dispersion relation, and normal modes

The linear stability analysis is performed by linearizing Eqs. (3) around the basic (OPO OFF) state (2) and considering normal modes solutions of the form $e^{ik_x x + ik_y y - i\omega t}$, where $\mathbf{k} = (k_x, k_y)$ is the *real* transverse wave vector and ω the complex frequency of the linear problem.

The pump variation is linearly decoupled from those of the signal and the idler, and the dispersion relation as obtained after straightforward calculations is

$$\mathcal{D}(k_x, k^2, \omega) = \omega^2 + i(b_s + b_i)\omega - b_s b_i + \gamma_s \gamma_i \mu^2 = 0, \quad (4)$$

where we have set

$$b_s = \gamma_s[1 + i(\Delta_s + a_s k^2 + \alpha_s k_x)],$$

$$b_i = \gamma_i[1 - i(\Delta_i + a_i k^2 - \alpha_i k_x)],$$

$$k^2 = k_x^2 + k_y^2.$$

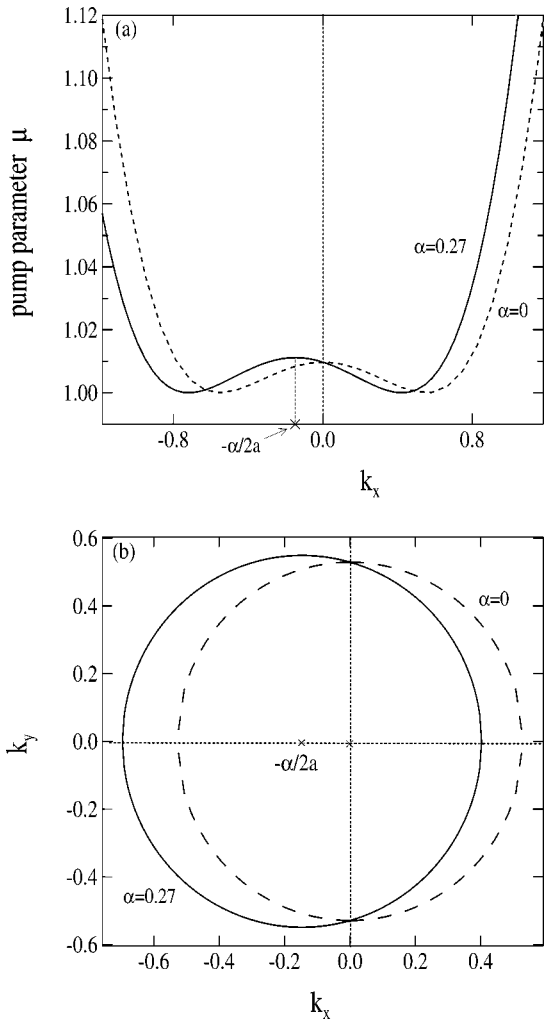

FIG. 1. The coupling effect between walkoff and diffraction breaks the rotational symmetry in the transverse plane. (a) Projection of the neutral stability surface on the (μ,k_x) plane. (b) Plot of the critical wave-vector components at the onset of instability ($\mu=\mu_c=1$). Walkoff shifts the circle of unstable transverse wave vectors. Signal walkoff parameter is $\alpha_s=0.27$ for the solid curves and $\alpha_s=0$ for the dashed ones. The fixed values, for all figures, of the other parameters are $\gamma_s=\gamma_i=1$, $\Delta_s=\Delta_i=-0.14$, $a_s=0.5$, $a_i=0.42$, and $\alpha_i=0$.

The dispersion relation yields the neutral stability surface $[\mathrm{Im}(\omega)=0]$ in the 2D plane of the wave-vector components (k_x,k_y) in the form

$$\mu(k_x,k_y)=\left(1+\frac{[\Delta-\alpha^2/4a+a(k_x+\alpha/2a)^2+ak_y^2]^2}{(\gamma_s+\gamma_i)^2}\right)^{1/2} \tag{5}$$

with a frequency

$$\omega(k_x,k_y)=\frac{\gamma_s\gamma_i}{\gamma_s+\gamma_i}[\Delta_s-\Delta_i+(a_s-a_i)k^2+(\alpha_s+\alpha_i)k_x],$$

where we have set $a=\gamma_s a_s+\gamma_i a_i$, $\Delta=\gamma_s\Delta_s+\gamma_i\Delta_i$, and $\alpha=\gamma_s\alpha_s-\gamma_i\alpha_i$. In the presence of walkoff, the critical surface (5) depends on both components of the wave vector (k_x,k_y), and cannot be reduced to a simple dependence on the wave-vector modulus $\mu(k^2)$, as is the case without walkoff [see Fig. 1(a) for a projection of this surface on the plane (μ,k_x)]. The stability analysis for the case $\Delta>0$ has been performed in [12]. In the sequel we will mainly focus on the case $\Delta<0$.

The onset of instability at critical threshold $\mu=\mu_c=1$ is obtained for wave vectors minimizing μ in Eq. (5) which are given by

$$(k_x^c+\alpha/2a)^2+(k_y^c)^2=\frac{\alpha^2-4a\Delta}{4a^2}. \tag{6}$$

The critical real wave vectors $\mathbf{k}^c=(k_x^c,k_y^c)$ belong to a circle [solid curve of Fig. 1(b)] centered at $(k_x=-\alpha/2a,k_y=0)$ with a radius $R=\sqrt{D}/2a$, and $D=\alpha^2-4a\Delta$. As indicated by the nonzero value of k_x, the rotational symmetry is broken by an amount $-\alpha/2a$ depending on the competition between walkoff and diffraction weighted by the cavity losses. Note that when walkoff vanishes [1], the circle (6) of critical wave vectors is centered on $\mathbf{k}=\mathbf{0}$, with $(k^c)^2=(k_x^c)^2+(k_y^c)^2=-\Delta/a$ [dashed curve of Fig. 1(b)]. The basic state (2) is linearly unstable to all 2D transverse modes lying on the circle (6). Contrarily to the case of positive effective detuning Δ, where walkoff selects at threshold a 1D structure expanding in its direction [12], this 1D selection mechanism fails for $\Delta<0$.

C. Response to localized perturbations

The linear stability analysis, given above, is based on the normal mode theory, i.e., it checks the stability with respect to extended perturbations. Such an approach is insufficient to determine the linear response of the system to any localized perturbation. This is provided by solving the linear initial-value problem:

$$\begin{aligned}
&\partial_t A_s-\gamma_s[-(1+i\Delta_s)A_s+\mu A_i^*+ia_s\nabla_\perp^2 A_s-\alpha_s\partial_x A_s]\\
&\quad=A_s^{(0)}\delta(x)\,\delta(y)\,\delta(t),\\
&\partial_t A_i^*-\gamma_i[-(1-i\Delta_i)A_i^*+\mu A_s-ia_i\nabla_\perp^2 A_i^*-\alpha_i\partial_x A_i^*]\\
&\quad=A_i^{*(0)}\delta(x)\,\delta(y)\,\delta(t).
\end{aligned} \tag{7}$$

The left-hand side is the linearized part of Eqs. (1) around the steady-state solution (2). The forcing terms added to the right-hand side of Eqs. (7) represent a localized initial impulse for A_s and A_i^*, δ being the Dirac function. Problem (7) can be solved using Fourier transforms in space (x,y) and the Laplace transform in time t, defined by

$$\begin{aligned}
\hat{\Phi}(k_x,k_y,\omega)=&\int_{-\infty}^{+\infty}\int_{-\infty}^{+\infty}\int_{0}^{+\infty}\Phi(x,y,t)\\
&\times e^{i(\omega t-k_x x-k_y y)}dx\,dy\,dt,
\end{aligned} \tag{8}$$

where $\Phi=(A_s,A_i^*,A_s^{(0)},A_i^{*(0)})^T$.

After solving the problem in Fourier space, and performing the Laplace transform by the residue theorem, the solution $A_s(x,y,t)$ may be written as

$$A_s(x,y,t) = -\frac{i}{4\pi^2}\sum_{n=1}^{2}\int_{-\infty}^{+\infty}\int_{-\infty}^{+\infty}\frac{S_n(\omega_n,k_x,k_y)}{\frac{\partial D}{\partial\omega}(\omega_n,k_x,k_y)} \times e^{-i(\omega_n t-k_x x-k_y y)}\, dk_x dk_y \tag{9}$$

with $S_n(\omega_n,k_x,k_y)=\hat{A}_s^{(0)}\{i\omega_n+\gamma_i[-(1-i\Delta_i)+ia_i k^2 - i\alpha_i k_x]\}-\gamma_s\mu\hat{A}_i^{*(0)}$, and ω_n $(n=1,2)$ are the two complex frequency modes solution of the dispersion relation (4). The mode, with the largest growth rate is the one which first absolutely destabilizes the system. Thus we shall now consider only this most destabilizing mode, whose frequency we will refer to as ω. The emerging signal pattern $A_s(x,y,t)$ is obtained by the asymptotic evaluation, as t tends to infinity, of the solution (9) along the rays $x/t=U$, $y/t=V$ for all constant values of U and V. Note that it is necessary to include x/t and y/t terms in order to allow the transverse point (x,y) to be large as t becomes large, so that one may follow a propagating perturbation. If the solution $A_s(x,y,t)$ is unbounded as $t\to\infty$, the system is linearly unstable, and then we have to distinguish between two types of instabilities. Any instability along a ray with $(U,V)=(0,0)$ grows in time *in situ* and invades the whole spatial domain: it is called ''absolute.'' Any instability along a ray with $(U,V)\neq(0,0)$ grows in time but is drifted away: it is called ''convective.'' Asymptotic expansions of the integral (9) can be obtained by applying the method of the steepest descent [18]. It consists, in particular, in deforming the real wave-vector k contour of integration in Eq. (9) into the two complex planes k_x and k_y without changing the value of the integral. The dominant part of the integrand arises in the region of the saddle point (k_x^s,k_y^s) defined by

$$\frac{\partial\omega}{\partial k_x}=U \quad \text{and} \quad \frac{\partial\omega}{\partial k_y}=V. \tag{10}$$

The shape of the signal response to the initial pulse perturbation is given in its dominant form by

$$A_s(x,y,t)\sim -\frac{i}{2\pi t}\frac{S(\omega(k_x^s,k_y^s),k_x^s,k_y^s)e^{i(k_x^s U+k_y^s V-\omega)t}}{\frac{\partial D}{\partial\omega}(k_x^s,k_y^s,\omega(k_x^s,k_y^s))\left[\left(\frac{\partial^2\omega}{\partial k_x\partial k_y}\right)^2-\frac{\partial^2\omega}{\partial k_x^2}\frac{\partial^2\omega}{\partial k_y^2}\right]^{1/2}_{(k_x^s,k_y^s)}}.$$

The necessary, but not sufficient, condition for absolute instability is the existence of a saddle point of frequency $\omega=\omega(k_x^s,k_y^s)$ in the two complex k_x and k_y planes for some complex $\omega^{(0)}$ with $\mathrm{Im}(\omega^{(0)})>0$ and $U=V=0$. However, for sufficiency, it is required that the spatial branches in each of the complex k_x and k_y planes, which are the solutions of the dispersion relation (4), originate from the real k_x axis and k_y axis. This is the so-called pinching condition [19]. These two points are investigated in the following. First, we look for the necessary condition, which provides us with possible values for the absolute instability threshold, and second we check the pinching condition for sufficiency.

Thus, the first step is to investigate the emergent signal (idler) pattern characteristics corresponding to the absolute instability at $U=V=0$, by solving

$$\frac{\partial\omega}{\partial k_x}=k_x F(k,k_x)+G(k,k_x)=U, \tag{11}$$

$$\frac{\partial\omega}{\partial k_y}=k_y F(k,k_x)=V, \tag{12}$$

with the ω solution of Eq. (4):

$$2\omega(k,k_x)=\overline{a}k^2+\overline{\alpha}k_x+\overline{\Delta}-i(\gamma_s+\gamma_i)+iR^{1/2}, \tag{13}$$

where

$$F=\overline{a}+a[\gamma_i-\gamma_s-i(ak^2+\alpha k_x+\Delta)]/R^{1/2},$$

$$2G=\overline{\alpha}+\alpha[\gamma_i-\gamma_s-i(ak^2+\alpha k_x+\Delta)]/R^{1/2},$$

$$R=4\gamma_s\gamma_i\mu^2+[\gamma_i-\gamma_s-i(ak^2+\alpha k_x+\Delta)]^2,$$

and

$$\overline{a}=\gamma_s a_s-\gamma_i a_i,$$

$$\overline{\Delta}=\gamma_s\Delta_s-\gamma_i\Delta_i,$$

$$\overline{\alpha}=\gamma_s\alpha_s+\gamma_i\alpha_i.$$

As can be seen from Eq. (12), $V=0$ when $k_y=0$ or $F(k,k_x)=0$. If $k_y\neq 0$, then the condition $(U,V)=(0,0)$ is fulfilled when $F(k,k_x)=G(k,k_x)=0$ which, after straightforward calculations, states $a_s\alpha_i+a_i\alpha_s=0$. Note that this coupling between drift and diffraction effects reduces to a vanishing walkoff condition in frequency-degenerated OPO's with negative signal detunings [5]. The condition $a_s\alpha_i+a_i\alpha_s=0$ requires very specific values of diffraction and walkoff, which are difficult to obtain experimentally. For the generic case $a_s\alpha_i+a_i\alpha_s\neq 0$ (which is always true in the

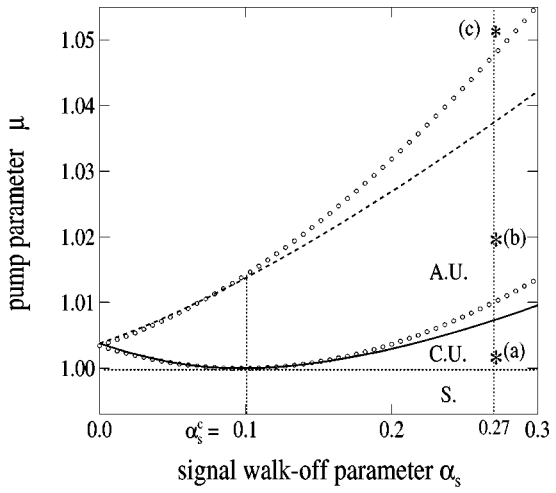

FIG. 2. Dependence of the pump parameter μ versus signal walkoff α_s at instability thresholds: solid curve for $\mu_{\rm abs}^-$ and dashed curve for $\mu_{\rm abs}^+$; both are obtained from the OPO dispersion relation. Open circles are the Ginzburg-Landau approximation. The OPO OFF solution is stable for $\mu<\mu_c=1$, convectively unstable for $\mu_c<\mu<\mu_{\rm abs}^-$, and absolutely unstable for $\mu>\mu_{\rm abs}^-$. The convective and absolute thresholds degenerate ($\mu_c=\mu_{\rm abs}^-$) at a critical value α_s^c: the system is then never convectively unstable.

case of degenerate OPO's with walkoff where $a_s=a_i$ and $\alpha_s=\alpha_i$), and then $(U,V)=(0,0)$ is satisfied for $k_y=0$. This means that the system selects the traveling waves propagating in the walkoff direction (x) among an infinity of unstable spatiotemporal modes. Two traveling waves (TW) with two different frequencies $\omega_\pm^{(0)}$ and wave vectors $(k_x^{s\pm},0)$ are selected at the different thresholds of absolute instability. To determine these thresholds $[\mu_{\rm abs}^\pm=\mu(k_x^{s\pm})]$, Eqs. (11) and (12), together with ${\rm Im}(\omega^{(0)})=0$ and $U=V=0$, have been numerically solved with a Newton-Raphson algorithm for a complex $\mathbf{k}^s=(k_x^s,0)$. The result of this integration $(\mu_{\rm abs}^\pm)$ is depicted in Fig. 2, which will be discussed in detail once the sufficient condition for absolute instability is verified.

The second step is to check that the frequencies of these two TW correspond to a pinching point in the k_x complex plane, i.e., the sufficient condition. To do this, we set $k_y=0$ in Eq. (13) and, by expanding it, obtain a fourth-degree polynomial of k_x. We then numerically solve it in the complex k_x plane by a Gauss-Laguerre method for different values of the pump parameter in the vicinity of the saddle point corresponding to $\alpha_s=0.27$.

For a given value of the pump parameter μ, the solution of the dispersion relation (4) forms four branches in the k_x space. The four branches for different values of the pump parameter μ are depicted in Fig. 3. As the pump parameter is increased, two branches emerge from the lower and from the upper half-planes, pinch below the real wave-vector axis when the saddle-point value is reached, and, finally, the usual exchange of branch identities is observed, as shown in Fig. 3. Note that the pinching condition is satisfied for both modes $\omega_-^{(0)}$ [Fig. 3(c)] and $\omega_+^{(0)}$ [Fig. 3(e)]. All saddle points we have numerically checked verify this sufficient condition.

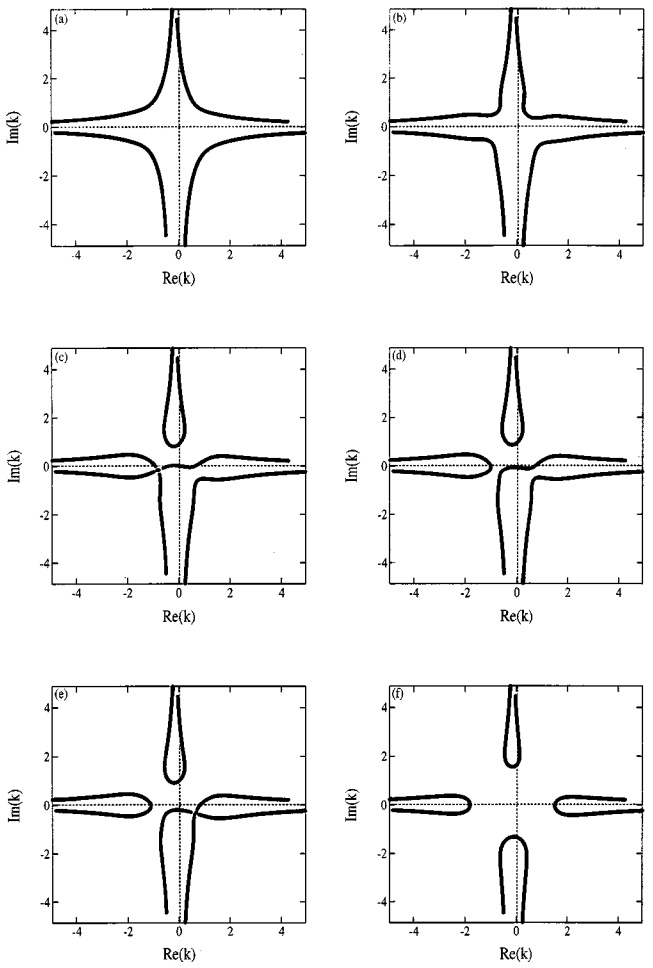

FIG. 3. The $\omega_i=0$ contours of the dispersion relation (4) are plotted in the complex k_x plane for increasing values of the pump parameter μ. (a) A contour with four branches is obtained for $\mu=0.5<\mu_{\rm abs}^-$, (b) $\mu=0.9<\mu_{\rm abs}^-$: the four branches are deformed. (c) $\mu=\mu_{\rm abs}^-=1.0075$: the branches ''pinch'' below the real axis for $k=k_{\rm abs}^-=(-0.82,-0.16)$. Note that ${\rm Re}(k_{\rm abs}^-)$ is negative. (d) $\mu_{\rm abs}^-<\mu=1.02<\mu_{\rm abs}^+$: the branches split and separate after pinching. (e) $\mu=\mu_{\rm abs}^+=1.038$: the pinching condition is fulfilled for $k=k_{\rm abs}^+=(+0.62,-0.33)$. Note that ${\rm Re}(k_{\rm abs}^+)$ is positive. (f) $\mu=1.5$: the branches split and separate again after pinching.

D. Discussion of the results

Let us now discuss the connection between our analysis and the mechanism of the transverse pattern formation when the pump parameter is varied. The variations of the absolute thresholds $\mu_{\rm abs}^\pm$ for both modes ω^+ and ω^- are plotted in Fig. 2 versus the walkoff parameter α_s in the case of a type-II OPO. They call for the following comments.

(i) $\mu_{\rm abs}^-$ (solid curve) exhibits a nontrivial dependence on walkoff in OPO's with negative detunings. The thresholds for absolute instabilities depend on a competition between walkoff and diffraction contrary to the threshold for convective instability $\mu_c=1$, which is independent of walkoff. The mode with frequency ω^- becomes absolutely unstable first regardless of the walkoff value. Thus at onset of the absolute instability, the system selects a TW propagating in the walkoff direction with a frequency $\omega_-^{(0)}$ and a wave number

$k^s(\omega_-^{(0)})$. Note that this is different (except for $\alpha=0$) from type-II degenerate OPO's as studied by Izùs *et al.* [9], where both modes have the same absolute threshold.

(ii) There exists a critical walkoff value α_s^c with particular properties. It corresponds to the minimum value of μ_{abs}^-, which is then equal to unity. This means that for $\alpha_s=\alpha_s^c$, both absolute and convective instability thresholds coincide. At this point, the OPO OFF state becomes directly absolutely unstable with no transition through a convective instability region as is observed for other values of the walkoff. This may be interpreted as the point of the strongest competition between walkoff and diffraction.

For $\alpha<\alpha_s^c$, the purely convective region ($1<\mu<\mu_{\text{abs}}^-$) shrinks as α_s is increased, meaning that the walkoff counterbalances diffraction, as far as instability thresholds are concerned. This occurs through a reduction of μ_{abs}^-, i.e., a lowering of the absolute instability threshold. For $\alpha>\alpha_s^c$, the absolute instability threshold increases with α_s, this is a parameter region where walkoff dominates diffraction.

In the general case of OPO's of both types, this occurs for parameter values Δ, α_j, and a_j linked by a relation analytically obtained by stating that at this point the group velocity of the most unstable mode vanishes, i.e., $(\partial\omega/\partial k)|_{k=k_c}=0$. This leads to the parameter relation

$$\Delta^c=-\{2\alpha(a_i-a_s)+a(\alpha_s+\alpha_i)\}\frac{(\alpha_s+\alpha_i)}{4(a_i-a_s)^2},$$

which is valid only for $a_s\neq a_i$.

Note that in all these expressions, the diffraction contribution is proportional to the difference between diffraction coefficients of the idler and signal fields (a_i-a_s). Therefore, it is expected that features such as the convective region in the absence of walkoff disappear in degenerate OPO's where $a_s=a_i$. This is similar to previous works on OPO's and degenerate OPO's in the absence of walkoff. For instance, Sanchez-Morcillo *et al.* [20] showed that in OPO's the localized structures have zero group velocity when $a_s=a_i$.

To summarize, in the general case, the existence of a convectively unstable regime stems from a complex competition between walkoff (α) and diffraction (a_i-a_s).

(iii) In the intermediate region $\mu_{\text{abs}}^-<\mu<\mu_{\text{abs}}^+$, it is expected that there will be a competition between the 1D absolute ω^- mode and the convective instability of the ω^+ mode since the pump parameter exceeds the threshold values for both these instabilities. To understand how the system destabilizes in these conditions, it is necessary to study the dynamics of the wave packets emerging from both transverse modes ω^- and ω^+.

III. EVOLUTION OF WAVE PACKETS IN THE UNSTABLE REGION

In the unstable regime, localized perturbations grow in space and time in the form of wave packets. Their evolution is characterized by their group velocity and their leading and trailing front velocities. The relevant wave packets are the ones which first destabilize the system and spread the fastest.

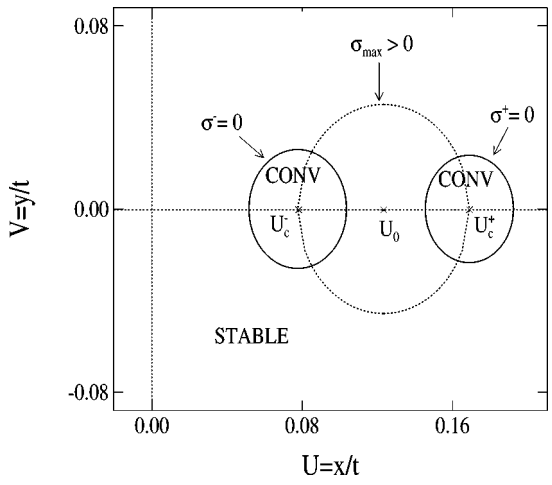

FIG. 4. The maximum growth rate ($\sigma_{\max}>0$) vs the group velocity (U,V) is depicted by the dashed line for a given pump parameter. The regions of convectively unstable 1D wave packets delimited by the solid line circle $\sigma^-=0$ ($\sigma^+=0$) centered on U_c^- (U_c^+) are also shown.

These relevant velocities can be obtained from the growth rate of unstable wave packets.

In this section, we first investigate the wave-packet propagation in the unstable regime and determine which mode first absolutely destabilizes the system, i.e., the first to have a vanishing leading front velocity. Second, nonlinear selection between the most unstable 1D modes is analyzed in terms of coupled amplitude equations, derived near threshold. We show that, in particular, nonlinear interaction prevents the occurrence of any mixed modes in the absolutely unstable regime.

A. Linear analysis of transverse wave packets

We restrict ourselves here to the case of wave packets with a positive growth rate $(\sigma\geqslant 0)$, i.e., above critical threshold $(\mu>\mu_c)$. Note that the temporal growth rate σ of the wave packet can easily be obtained from Eq. (9) as $\sigma=\omega_i-\text{Im}(k_x)U-\text{Im}(k_y)V$. It takes into account, in addition to the usual temporal growth term ω_i, spatial contribution terms where the propagation velocity (U,V) of a wave packet has an important role in the unstable region $(\sigma\geqslant 0)$. Let us recall that when the instability is convective, then the origin $(U,V)=(0,0)$ does not belong to the unstable wave packet. The instability becomes absolute when the wave packet spreads but at least one spatial mode has a vanishing front velocity (U,V). It is thus natural to determine the convective/absolute nature of an unstable wave packet by characterizing the evolution of its temporal growth rate in the (U,V) plane. The critical velocities of the most destabilizing wave packets, at criticality $(\mu=\mu_c)$ where they reach their greatest growth rate, are defined by $\sigma_{\max}=\sigma(\omega_c,\mathbf{k}_c,(U_c,V_c))$ with $(U_c,V_c)=\overset{\text{grad}}{\rightarrow}_{\mathbf{k}}\omega_r|_c$. After simple calculations, they are analytically given by

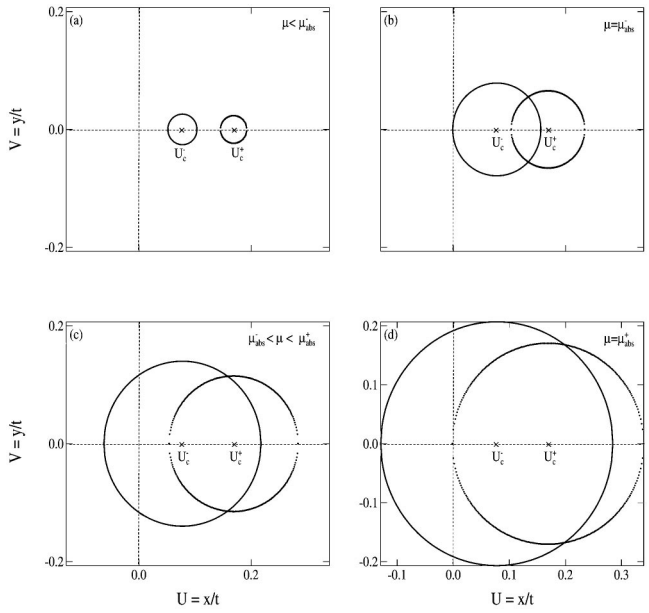

FIG. 5. Transition from convective to absolute instability of the two most unstable 1D wave packets of Fig. 4 is illustrated, for different values of the pump parameter μ, in the (U,V) plane. (a) $\mu<\mu_{\rm abs}^{-}$ reproducing the two small circles of Fig. 4. (b) At $\mu=\mu_{\rm abs}^{-}$, one of the circles (σ^{-}) touches the origin: the system becomes absolutely unstable. (c) $\mu_{\rm abs}^{-}<\mu=1.02<\mu_{\rm abs}^{+}$ for all values of (U,V) inside the circle (σ^{-}), the system is absolutely unstable. (d) $\mu=\mu_{\rm abs}^{+}=1.1$ and the circle (σ^{+}) in turn touches the origin leading to the absolute instability of the second transverse mode ω^{+}.

$$\mathbf{v}_c=\left\{(U_c,V_c)\ \text{ such that } (U_c-U_c^0)^2+V_c^2 =R_c^2=[(a_s-a_i)/\tau]^2\left(\frac{D}{4a^2}\right)\right\},$$

where $U_c^0=\gamma_s\gamma_i(a_s\alpha_i+a_i\alpha_s)/(a_s\gamma_s+a_i\gamma_i)$. The set $\mathbf{v}_c$ corresponds, in the plane (U,V), to a circle centered at $(U=U_c^0,V=0)$ and with a radius R_c. For fixed parameters, at threshold $\mu=\mu_c$, each point on the circle represents a defined group velocity from which 2D wave packets emerge for $\mu>\mu_c$. These group velocities, in the presence of walkoff, are at unequal distances from the origin $(U,V)=(0,0)$. For $\mu>\mu_c$, the unstable wave packets expand, in the unstable region $(\sigma\geqslant 0)$, and their trailing fronts are limited by the zero growth rate $\sigma=0$. Figure 4 shows, in the (U,V) plane, the circle $(\mathbf{v}_c)$ of critical velocities. Only the emerging wave packets from the two 1D modes $\mathbf{k}_c^{\pm}=(k_c^{\pm},0)$ are shown, for clarity. Their respective convectively unstable regions $[\sigma\geqslant 0$ and $(U,V)\neq(0,0)]$ limited by the circles $\sigma^{\pm}=\sigma(k_c^{\pm})=0$ are also shown. When increasing the value of μ above μ_c, one of the infinity of wave packets centered on the circle $(\mathbf{v}_c)$ will reach the origin first leading to the onset of absolute instability. As a consequence, the selected wave packet is the one closest to the origin, which is the one with the smallest group velocity on the U_c axis with $V_c=0$. Hence, the most absolutely unstable mode is that of the two modes $\mathbf{k}_c^{\pm}=(k_c^{\pm},0)$ having the smaller velocity $U_c^{\pm}$ (see Fig. 4). Therefore, among all 2D convective unstable modes, above critical threshold $(\mu>\mu_c)$, one may only deal with those active modes lying near the 1D critical modes $\mathbf{k}_c^{\pm}=(k_c^{\pm},0)$ parallel to the walkoff. We will thus carry out a 2D analytical study of the propagating wave packets, resulting from the competition between these 1D transverse modes given by

$$\mathbf{k}_c^{\pm}=(k_c^{\pm},0)\quad\text{with}\quad k_c^{\pm}=(-\alpha\pm\sqrt{D})/2a,$$
$$\omega_c^{\pm}=\omega_0-U_c^0k_c^{\pm}, \tag{14}$$

with $\omega_0=[\Delta_i-\Delta_s+(a_s-a_i)\Delta/a]/2\tau=\omega_c^{\pm}(\alpha_s=\alpha_i=0)$. The maximum growth rate $\sigma_{\max}$ is reached for $U_c^{\pm}=U_c^0\pm(a_s-a_i)\sqrt{D}/2a\tau$ while $V_c^{\pm}=0$. To determine the front velocity U, we once again use the Newton-Raphson algorithm. Figure 5 shows the result of the integration of the OPO dispersion relation (4) under the condition $\sigma=0$, in the plane (U,V), and for increasing values of the pump parameter μ. At threshold of convective instability $(\mu=\mu_c)$, $\sigma_{\max}=0$ and corresponds to two points (crosses in Fig. 5) in the plane (U,V). Above onset at $\mu>\mu_c$, $\sigma_{\max}$ is positive and all positive σ such that $0<\sigma<\sigma_{\max}$ belong to the disks delimited by $\sigma=0$ circles. The velocities (U^*,V^*) corresponding to $\sigma=0$ represent 2D fronts of the perturbations, so along these rays $(x/t=U^*$ and $y/t=V^*)$ the system is marginally stable. At some pump parameter $\mu=\mu_{\rm abs}>\mu_c$, $U^*=V^*=0$, and the system becomes absolutely unstable [Fig. 5(b) and Fig. 5(d)]. It is clear that the mode ω^{-} becomes absolutely unstable before the mode ω^{+} as can be seen from these figures.

The curves in Fig. 5(b) and Fig. 5(c) also show that while the mode ω^{-} is absolutely unstable, the mode ω^{+} is still convectively unstable since the corresponding disk does not contain the origin. For $\mu>\mu_{\rm abs}^{+}$, the system is absolutely unstable with respect to the two modes ω^{+} and ω^{-} [Fig. 5(d)]. The fastest front velocity linearly takes over the dynamics of the system.

In order to study the nonlinear coupling between these two modes, we derive amplitude equations close to critical threshold. We restrict ourselves to a 1D weakly nonlinear analysis of these two modes, since the first mode to be absolutely selected is 1D, and is the first to be affected by the nonlinear saturation.

B. Nonlinear wave-packet selection

The wave packets centered on the unstable modes ω_c^{+} and ω_c^{-} can be characterized as plane waves $S_{\pm}(x,t)\exp i(k_c^{\pm}x-\omega_c^{\pm}t)$, respectively, with complex amplitudes $S_{\pm}(x,t)$ which may be slowly modulated in space and time. The weakly nonlinear dynamics of these wave packets can be described by a set of two coupled complex Ginzburg-Landau equations (CCGLE) for the amplitudes $S_{\pm}$ (see the Appendix for details). Their 1D version reads

$$\tau(\partial_t + U_c^+ \partial_x)S_+ = (\mu-1)S_+ + (d_1+id_2)\partial_x^2 S_+ - [N|S_+|^2 + (N+C^+)|S_-|^2]S_+, \tag{15}$$

$$\tau(\partial_t + U_c^- \partial_x)S_- = (\mu-1)S_- + (d_1+id_2)\partial_x^2 S_- - [N|S_-|^2 + (N+C^-)|S_+|^2]S_-, \tag{16}$$

with all coefficients defined in the Appendix.

Note that contrary to the classical CCGLE, the presence of the walkoff, which breaks the reflection symmetry ($x \leftrightarrow -x$), compels the group velocities ($U_c^{\pm}$) and the nonlinear cross-coupling terms ($N+C^{\pm}$) to take different values for each mode (S_+ and S_-). We first calculate the boundary for absolute instability within the context of linear parts of Eqs. (15) and (16). This linear problem can be solved by exact integration for an initial condition of the form $S_{\pm}(x,t=0) = \delta(x)$ (a Dirac function), giving for $t>0$ [21]

$$S_{\pm} = \left[\frac{4\pi}{\tau}(d_1+id_2)t\right]^{-1/2} \times \exp\left[\frac{\mu-1}{\tau}t - \tau(d_1-id_2)\frac{(x-U_c^{\pm}t)^2}{4(d_1^2+d_2^2)t}\right]. \tag{17}$$

In the limit of long time behavior, the growth rate $\sigma_{\pm}$ of the amplitudes $S_{\pm}$ for any position x reads

$$\sigma_{\pm} = \frac{\mu-1}{\tau} - \tau d_1 \frac{(x/t - U_c^{\pm})^2}{4(d_1^2+d_2^2)}. \tag{18}$$

In the frame moving at velocity $(x/t)^{\pm} = U_c^{\pm}$, the amplitudes $S_{\pm}$ are dominated by the most unstable modes with the maximum growth rate $\sigma_{\pm}^{\max}$ reducing to $(\mu-1)/\tau$. A wave packet that eventually grows in some frame is confined between two rays on which the growth rate is zero. In order to obtain the absolute instability boundary, we take $\sigma=0$ at a fixed point (i.e., $x/t=0$). The onset for absolute instability then reads

$$\mu_{\rm abs}^{\pm} = 1 + \frac{\tau^2 d_1}{4(d_1^2+d_2^2)}(U_c^{\pm})^2. \tag{19}$$

The boundary $\mu_{\rm abs}^{\pm}$ is plotted versus α_s as open circles in the stability diagram of Fig. 2. As can be seen from this plot, the CCGLE approximation is valid in the whole range of accepted values of walkoff and the accuracy is excellent for small ones.

In order to determine the wave number and the frequency of the two respective modes at their absolute threshold, we perform a saddle-point analysis [12] in the context of linear parts of Eqs. (15) and (16). A straightforward calculation leads to

$$k_s^{\pm} = k_c^{\pm} - \frac{\tau(d_1+id_2)U_c^{\pm}}{2(d_1^2+d_2^2)}, \tag{20}$$

$$\omega_s^{\pm} = \omega_c^{\pm} - \frac{\tau(U_c^{\pm})^2}{4(d_1^2+d_2^2)}, \tag{21}$$

with $k_c^{\pm} = (-\alpha \pm \sqrt{D})/2a$ and $\omega_c^{\pm} = \omega_0 - k_c^{\pm}U_c^0$.

A short inspection of the relations (19)–(21) and of the stability diagram of Fig. 2 shows that when the walkoff vanishes, the two modes S_+ and S_- simultaneously become absolutely unstable. They correspond to traveling waves propagating in opposite directions with velocities $U_c^{\pm}(\alpha_s = \alpha_i = 0) = \pm(a_s - a_i)\sqrt{D}/(2\tau a)$. So we can say that the system exhibits bicritical absolute instability. In the presence of walkoff, this bicriticality persists for degenerate OPO's where $a_s = a_i$ [9]. These systems may exhibit at the absolute instability threshold, according to the linear analysis, two traveling waves propagating in the same direction with the same velocity $U_c^{\pm}(a_s=a_i) = U_c^0 = \gamma_s\gamma_i(a_s\alpha_i + a_i\alpha_s)/(a_s\gamma_s + a_i\gamma_i)$ but different wave numbers and frequencies. The situation is qualitatively different for OPO's. The presence of walkoff breaks the bicritical nature of the absolute instability and the two modes S_+ and S_- may appear at different absolute instability thresholds (Fig. 2). The physical parameters chosen in the numerical simulations imply that the mode S_- appears first (i.e., $\mu_{\rm abs}^- < \mu_{\rm abs}^+$). All these predictions are associated with the linear properties in the sense that only the nature of the instability of the trivial homogeneous and time-independent solution (OPO OFF) was investigated. A nonlinear analysis is required to clarify which pattern may be selected when the system becomes absolutely unstable. Equations (15) and (16) admit spatially uniform, time-independent solutions: (0,0), (S_-^s,0), (0,S_+^s), and the mixed mode (S_-^m,S_+^m), such that $|S_-^s|^2 = |S_+^s|^2 = (\mu-1)/N$ and $|S_-^m|^2 = (\mu-1)C^-/[N(C^+ + C^-) + C^-C^+]$; $|S_+^m|^2 = |S_-^m|^2 C^+/C^-$. We note that C^+ and C^- are different, so that the system does not allow for standing waves. The above linear spatiotemporal analysis showed that the trivial state (0,0) becomes absolutely unstable when $\mu > \mu_{\rm abs}^-$. As a consequence, the traveling wave with the amplitude S_- spreads over the whole spatial domain. As the pumping is increased, the question of the transition from this traveling wave to the mixed ones with amplitudes (S_-^m,S_+^m) remains. The study of the stability of the mode (S_-^s,0) with respect to mixed modes is then required. It is done by introducing the perturbed amplitudes $S_-(x,t) = S_-^s + \delta S_-^s(x,t)$ and $S_+(x,t) = \delta S_+(x,t)$, and performing a linear stability analysis. This leads to two eigenvalues, which can be related to amplitude and phase disturbances, respectively. The amplitude ones never destabilize $S_-(x,t)$ since their growth rate $\sigma_{\rm amp} = -2(\mu-1)/(N\tau)$ is negative. The growth rate of the phase disturbances $\sigma_\varphi = -(Nd_1/\tau)q^2 - O(q^4)$ is also negative (q being the wave number of the perturbation). Therefore, the system does not experience the Benjamin-Feir instability. Up to now, we have considered a traveling wave with wave number $k = k_c^-$ (i.e., S_-^s is homogeneous). If the wave number k

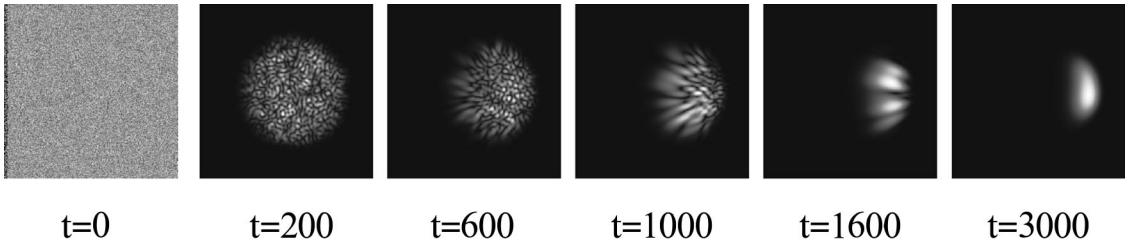

FIG. 6. Time evolution of the near-field signal amplitude obtained from the integration of the full 2D OPO model. The pump parameter value is that of point (a) in Fig. 2, where the system is convectively unstable.

is allowed to vary ($k \neq k_c$), we expect that the traveling wave may experience the Eckhaus and zigzag instabilities. The study of the convective or absolute nature of these secondary instabilities is worth addressing. Work in this direction is in progress. Thus the stability of the mode (S_-^s,0) depends only on the stability of the traveling wave $S_+(x,t)$. By linearizing Eq. (15), one gets

$$\tau(\partial_t + U_c^+ \partial_x)\delta S_+(x,t) = (\mu - 1)\delta S_+(x,t) + (d_1 + id_2)\partial_x^2 \delta S_+(x,t) - (N + C^+)|S_-^s|^2 \delta S_+(x,t).$$

If we consider the expression of $|S_-^s|^2 = (\mu - 1)/N$, the effective growth rate of $\delta S_+(x,t)$ is found to be $(\mu - 1)(-C^+/\tau N)$. We note that the presence of the cross-coupling term (C^+) leads to a nonlinear negative growth rate for the mode S_+. Therefore, we do not expect any transition from the S_-^s mode to the mixed mode in this problem. Hence, the upper curve in Fig. 2 has no physical meaning because it does not take into account the nonlinear interaction between the two unstable modes. We finally state that this nonlinear selection and the importance of the coupling terms in Eqs. (15) and (16) also hold for the bicritical absolute instability present in particular, in degenerate OPO's. Indeed, if for a range of initial conditions one of the two modes is excited and spreads over the whole spatial domain, no transition to the mixed modes is predicted by our nonlinear stability analysis. This result is consistent with numerical simulations of degenerate OPO equations reported in [9].

IV. NUMERICAL RESULTS

In this section, we numerically investigate the validity of our predictions by integrating the full 2D OPO model [Eqs. (1)] above the critical threshold ($\mu = \mu_c$). For the integration we use the same scheme as in [8]. We just recall here that the integration is based on a variable-step fourth-order Runge-Kutta algorithm for the temporal evolution in normalized γ_s units. The variables are developed on a 256×256 grid of 240 spatial units, performing the diffraction terms calculation by means of a fast Fourier transformation into $\mathbf{k} = (k_x, k_y)$ space and back. For the external pump, we used a Gaussian beam

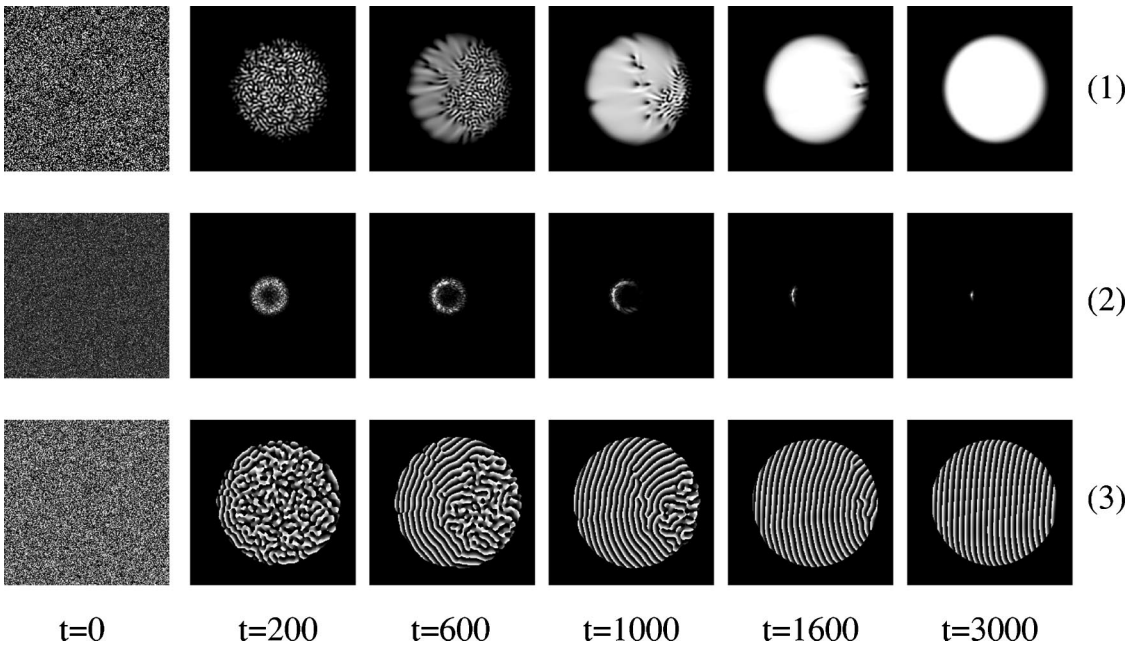

FIG. 7. Time evolution of the signal field pattern in the absolutely unstable regime [point (c) in Fig. 2]. (1) Amplitude time evolution in the real transverse plane (near-field). (2) The far-field evolution. Note that the wave vector selected is negative. (3) Phase pattern evolution towards a stripe pattern.

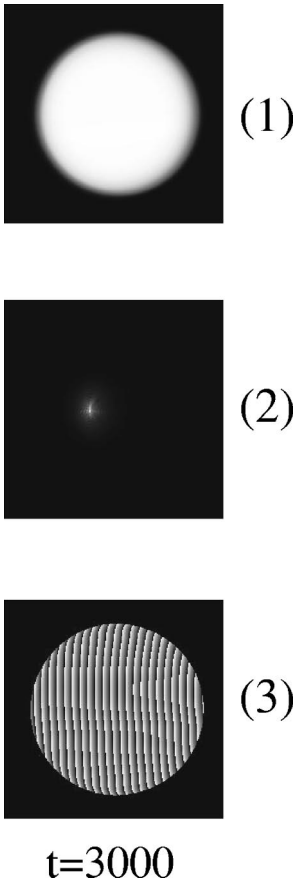

FIG. 8. The asymptotic signal field ($t=3000$) for $\mu=1.05>\mu_{\rm abs}^{+}$ is plotted. (1) Near field, (2) far field, and (3) phase pattern. Note that the numerically selected wave vector in (2) is negative, as predicted by the nonlinear stability analysis.

of maximum amplitude E_0 and with a waist of 112 units, while the signal and idler fields are generated starting from random initial conditions [8]. The evolution of the transverse dynamics is computed for a fixed signal and idler pair of walkoff parameters α_s and α_i and various pump parameter values above the instability threshold. The numerical solutions presented here are obtained for a type-II OPO with $\alpha_s=0.27$ and $\alpha_i=0$. The choice of the value of α_s corresponds to a walkoff angle of about 0.1 mrad for the signal field and was discussed in [8] in connection with experiments. The remaining parameters are set to $\gamma_p=\gamma_s=\gamma_i=1$, $\Delta_p=2$, $\Delta_s=\Delta_i=-0.14$, $a_p=0.23$, $a_s=0.5$, and $a_i=0.42$.

Here we have reported three series of numerical solutions of Eqs. (1) representative of the three qualitatively different regions of Fig. 2, namely (i) $\mu_c=1<\mu<\mu_{\rm abs}^{-}$, where the OPO is convectively unstable; (ii) $\mu_{\rm abs}^{-}<\mu<\mu_{\rm abs}^{+}$, where the system is globally absolutely unstable with respect to the ω^{-} mode; and (iii) $\mu>\mu_{\rm abs}^{+}$, where both transverse modes are linearly absolutely unstable. In the first region (i) and for $E_0=2.24$ [corresponding to $\mu\simeq1.002$, point (a) in Fig. 2], the temporal evolution of the signal field pattern is shown in Fig. 6, starting from random initial conditions. In the transient regime ($t\lesssim600$), we observe the random formation of domains in the amplitude of the signal field where all linear active modes are present. Later, the defects or inhomogeneous wave packets which are randomly distributed in the signal amplitude propagate from the left to the right in the direction of the walkoff, i.e., in one direction only, and are drifted outside the transverse pump section giving rise, at long time ($t=3000$), to a front which eventually disappears.

By further increasing the pump parameter, we enter the region (ii) where the mode ω^{-} is absolutely unstable, as shown in Fig. 7, for $E_0=2.28$ [$\mu\simeq1.02>\mu_{\rm abs}^{-}$; point (b) in Fig. 2]. The most significant feature is that the generated transverse signal beam (upper row) extends asymptotically all over the pump transverse section, therefore increasing the OPO efficiency together with the energy conversion from the pump to the signal. The far-field (middle row) and the phase pattern (bottom row) evolution are also shown in this figure. The formation of the ring of linearly unstable transverse modes in the far-field and the corresponding phase patterns is seen for early time development ($t\lesssim600$). The further time evolution ($600\lesssim t\lesssim1600$) shows the nonlinear selection where only those 2D modes lying near the most absolutely unstable mode ω^{-} are still active, as predicted in Sec. III. As can be seen from the figure, the asymptotic state corresponds to a signal field with homogeneous amplitude and a phase stripe pattern, perpendicular to the walkoff direction. The wave number of the stripe pattern is equal to that predicted [see Fig. 3(c)] by the linear absolute stability analysis.

When the pump parameter μ exceeds the absolute threshold $\mu_{\rm abs}^{+}$ of the mode ω^{+}, the linear stability analysis states that both modes with negative (respectively positive) wave number for the ω^{-} (ω^{+}) mode could develop, as shown in Fig. 3(c) [respectively Fig. 3(e)]. A typical asymptotic numerical solution is depicted in Fig. 8 for a pump parameter value $E_0=2.35$ [$\mu\simeq1.05$; point (c) in Fig. 2] above the absolute threshold $\mu_{\rm abs}^{+}$. The OFF state is destabilized all over the transverse profile and the OPO emits a circular bright spot. Note that on the far-field image of Fig. 8, the wave number is negative. This is in agreement with the nonlinear analysis, which predicts that even in the region where the mode ω^{+} is *linearly absolutely* unstable, it is the mode ω^{-} which is selected. Indeed, once the first unstable mode (ω^{-}) is present, it inhibits all other linearly active modes. The emerging pattern depends strongly on the nonlinear interaction among all active modes. This is exactly what we have observed in Fig. 8. Let us recall that this is different from the case of degenerate OPO's where both modes (ω^{-} and ω^{+}) have the same linear absolute growth rate, which is selected depending only on the initial conditions [9].

V. CONCLUSION

Transverse pattern formation in OPO's as a response of a 2D localized perturbation has been examined. As far as we consider localized perturbations, the transverse asymptotic form of the signal is given by the ''modes'' evaluated with complex wave vectors, and not with real-valued wave vectors. These wave vectors correspond to the saddle points of the OPO dispersion relation. It turns out that, at the onset of instability, in nondegenerate OPO's, a ring of wave vectors is excited giving rise to propagating wave packets but with *different* group velocities. In the absence of a noise source,

these wave packets are drifted outside the transverse gain section of the pump field which is at rest and no long-term pattern is observed. The system settles back to the basic state (OPO OFF). A small increase in the pump parameter brings the system into an absolutely unstable regime where the group velocity vanishes for, at least, one of the wave packets which grows in place invading the whole available transverse section. Two parameters play a key role in the respective position of the thresholds, namely the walkoff parameter and the diffraction asymmetry $a_i - a_s$. Walkoff is known to introduce a drift, but it is important to mention the counterdrift due to diffraction asymmetry. In particular, the convective instability region may disappear when this diffraction asymmetry compensates for walkoff. We have also demonstrated that the system selects only two asymmetric 1D spatial structures, with different wave vectors aligned in the walkoff direction, but with two distinct absolute thresholds. Because of the nonlinear interaction of these two modes, only one of them (the one with the lower linear absolute threshold) is systematically selected, irrespective of the initial conditions. All analytical predictions have been confirmed by integrating numerically the full 2D OPO model.

We have limited this work to primary instabilities. However, in a certain range of parameters, the wave packets may be destabilized either in phase or in amplitude and secondary instabilities should be investigated. In particular, the impact of convective and absolute instabilities on the thresholds of Eckhaus and zigzag instabilities is worth examining in order to understand the pattern formation of OPO's for higher values of the pump parameter. Work in this direction is in progress.

ACKNOWLEDGMENTS

The authors acknowledge helpful discussions with M. San Miguel, M. Santagiustina, and A. Barsella. One of us (M. N. O.) acknowledges A. Couairon and J. M. Chomaz for stimulating discussions. The Laboratoire de Physique des Lasers, Atomes et Molécules is ''Unité Mixte de Recherche du Center National de la Recherche Scientifique.'' The Center d'Etudes et de Recherches Lasers et Applications (CERLA) is supported by the Ministère Chargé de la Recherche, the Région Nord/Pas de Calais, and the Fonds Européen de Développement Economique des Régions.

APPENDIX

In the following, we present the derivation of the coupled Ginzburg-Landau amplitude equations from the mean-field model of the OPO. For this purpose, it is worthwhile to write the OPO equations (1) in the compact notation

$$\partial_t V = LV + N, \tag{A1}$$

where the vector $V=(B,A_s,A_i^*)^T$ contains the three field variables, * stands for the complex conjugate, and L is the linear operator of the system,

$$L=\begin{pmatrix} -\gamma_p(1+i\Delta_p)+i\gamma_p a_p\nabla_\perp^2 & 0 & 0 \\ 0 & -\gamma_s(1+i\Delta_s)+i\gamma_s a_s\nabla_\perp^2-\gamma_s\alpha_s\partial_x & \mu\gamma_s \\ 0 & \mu\gamma_i & -\gamma_i(1-i\Delta_i)-i\gamma_i a_i\nabla_\perp^2-\gamma_i\alpha_i\partial_x \end{pmatrix}.$$

N is the nonlinear operator,

$$N=\begin{pmatrix} -\gamma_p A_s A_i \\ \gamma_s A_i^* B \\ \gamma_i A_s B^* \end{pmatrix}.$$

At threshold (for $\Delta=\gamma_s\Delta_s+\gamma_i\Delta_i<0$), the linear stability analysis [12] shows that the OPO presents a supercritical bifurcation at $\mu=\mu_c=1$ to a nonhomogeneous state (k_c,ω_c) defined by

$$k_c^{\pm}=\pm\frac{\sqrt{D}}{2a}-\frac{\alpha}{2a},$$

$$\omega_c=\omega_c^{(0)}-U_c^0 k_c^{\pm},$$

where we have set $\alpha=\alpha_s\gamma_s-\alpha_i\gamma_i$, $a=a_s\gamma_s+a_i\gamma_i$, and $D=\alpha^2-4a\Delta$ in the first equation. In the second one, $\omega_c^{(0)}=\gamma_s\gamma_i[\Delta_i-\Delta_s-\Delta(a_i-a_s)/a]/(\gamma_s+\gamma_i)$ is the critical frequency in the absence of walkoff and $U_c^0=\gamma_s\gamma_i(a_s\alpha_i+a_i\alpha_s)/a$. Above threshold, we introduce a small parameter ε which measures the distance to criticality by setting $\mu-\mu_c=\varepsilon^2\mu_2$, where μ_2 is of order unity. This fixes the spatial and temporal scalings to (see Refs. [1,12])

$$\begin{aligned} x&=X_0+\varepsilon X, \\ y&=Y_0+\sqrt{\varepsilon}Y, \\ t&=T_0+\varepsilon T_1+\varepsilon^2 T_2+\cdots. \end{aligned} \tag{A2}$$

Temporal and spatial derivatives in Eqs. (1) are then replaced by

$$\begin{aligned} \partial_t&=\partial_{T_0}+\varepsilon\partial_{T_1}+\varepsilon^2\partial_{T_2}, \\ \partial_x&=\partial_{X_0}+\varepsilon\partial_X, \\ \partial_y&=\partial_{Y_0}+\sqrt{\varepsilon}\partial_Y. \end{aligned} \tag{A3}$$

The evolution equations for the field variables are obtained by expanding the solution V in power series of ε:

$$V=\varepsilon V^{(1)}+\varepsilon^2 V^{(2)}+\varepsilon^3 V^{(3)}\cdots. \tag{A4}$$

The functions $V^{(i)}$ depend on the slow variables X, Y, T_1, and T_2. By substituting the expansion (A4) and the relations (A3) and (A2) in Eqs. (1), and then collecting coefficients of like powers of ε, the following equations are obtained:

$$\begin{aligned}
&(\partial_{T_0}-L_0)V^{(1)}=0, && O(\varepsilon),\\
&(\partial_{T_0}-L_0)V^{(2)}=(-\partial_{T_1}+L_1)V^{(1)}+N^{(2)}, && O(\varepsilon^2),\\
&(\partial_{T_0}-L_0)V^{(3)}=(-\partial_{T_1}+L_1)V^{(2)}+(-\partial_{T_2}+L_2)V^{(1)}+N^{(3)}, && O(\varepsilon^3),
\end{aligned} \tag{A5}$$

where L_0 is the linear operator of the system for $\mu=\mu_c=1$, and L_1, and L_2 are defined by

$$L_1=\begin{pmatrix} i\gamma_p a_p(2\partial^2_{X_0X}+\partial^2_Y) & 0 & 0\\ 0 & i\gamma_s a_s(2\partial^2_{X_0X}+\partial^2_Y)-\gamma_s\alpha_s\partial_X & 0\\ 0 & 0 & -i\gamma_i a_i(2\partial^2_{X_0X}+\partial^2_Y)-\gamma_i\alpha_i\partial_X \end{pmatrix},$$

$$L_2=\begin{pmatrix} i\gamma_p a_p\partial^2_X & 0 & 0\\ 0 & i\gamma_s a_s\partial^2_X & \gamma_s\mu_2\\ 0 & \gamma_i\mu_2 & -i\gamma_i a_i\partial^2_X \end{pmatrix}.$$

$N^{(2)}$ and $N^{(3)}$ are the nonlinear terms.

At $O(\varepsilon)$ we find that

$$V^{(1)}=\begin{pmatrix}0\\1\\1\end{pmatrix}A_\pm(X,Y,T_1,T_2)e^{i(k_c^\pm x+\omega_c^\pm T_0)},$$

where we take the convention of writing

$$A_\pm e^{i(k_c^\pm x+\omega_c^\pm T_0)}=A_+e^{i(k_c^+x+\omega_c^+T_0)}+A_-e^{i(k_c^-x+\omega_c^-T_0)}.$$

Applying the solvability condition at order $O(\varepsilon^2)$ leads to

$$\partial_{T_1}A_\pm=\frac{1}{\tau}\left[\left([a_i-a_s]k_c^\pm-\frac{\alpha_s+\alpha_i}{2}\right)\partial_X A_\pm+\frac{i}{2}(a_s-a_i)\partial_Y^2A_\pm\right], \tag{A6}$$

where $\tau=(\gamma_s+\gamma_i)/2\gamma_s\gamma_i$.

The equation at this order has then a solution $V^{(2)}=(B_2,A_s^\pm,0)^T$, where

$$B_2=-\frac{|A_\pm|^2}{1+i\Delta_p}-\frac{\gamma_pA_\pm A_\mp^* e^{i[(\pm k_c^+\mp k_c^-)x+(\pm\omega_c^+\mp\omega_c^-)T_0]}}{\gamma_p+i[\gamma_p\Delta_p+\gamma_pa_p(k_c^+-k_c^-)^2+(\pm\omega_c^+\mp\omega_c^-)]},$$

$$(\gamma_i+\gamma_s)A_s^\pm=[-(2ak_c^\pm+\alpha)\partial_X+ia\partial_Y^2]A_\pm e^{i(k_c^\pm x+\omega_c^\pm T_0)}.$$

Similarly, applying the solvability condition at $O(\varepsilon^3)$ yields, in terms of the original space and time variables,

$$\begin{aligned}
\tau(\partial_t+U_c^+\partial_x)S_+=&(\mu-1)S_++i\frac{a_s-a_i}{2}\nabla_\perp^2S_+\\
&-\Lambda\left[2i\left(k_c^++\frac{\alpha}{2a}\right)\partial_x+\partial_y^2\right]^2S_+\\
&-[N|S_+|^2+(N+C^+)|S_-|^2]S^+,
\end{aligned} \tag{A7}$$

$$\begin{aligned}
\tau(\partial_t+U_c^-\partial_x)S_-=&(\mu-1)S_-+i\frac{a_s-a_i}{2}\nabla_\perp^2S_-\\
&-\Lambda\left[2i\left(k_c^-+\frac{\alpha}{2a}\right)\partial_x+\partial_y^2\right]^2S_-\\
&-[N|S_-|^2+(N+C^-)|S_+|^2]S^-,
\end{aligned} \tag{A8}$$

where

$$\tau=\frac{\gamma_s+\gamma_i}{2\gamma_s\gamma_i},$$

$$U_c^\pm=(a_s-a_i)k_c^\pm/\tau+\frac{\alpha_s+\alpha_i}{2\tau}=\pm(a_s-a_i)\sqrt{D}/2\tau a+\gamma_s\gamma_i\frac{a_s\alpha_i+a_i\alpha_s}{a},$$

$$\Lambda=\frac{1}{2}\left(\frac{a}{\gamma_s+\gamma_i}\right)^2,$$

$$N=\frac{1}{1+\Delta_p^2},$$

$$\frac{1}{C^{\pm}}=1+\left[\Delta_p+D\frac{a_p}{a^2}\mp\frac{\gamma_s\gamma_i}{\gamma_p}\frac{a_s\alpha_i+a_i\alpha_s}{a}\frac{\sqrt{D}}{a}\right]^2.$$

Notice that, by dropping all y derivatives in the above amplitude equations, one gets their 1D version, parallel to the walkoff direction x, as

$$\tau(\partial_t+U_c^+\partial_x)S_+=(\mu-1)S_++(d_1+id_2)\partial_x^2S_+ -[N|S_+|^2+(N+C^+)|S_-|^2]S_+, \tag{A9}$$

$$\tau(\partial_t+U_c^-\partial_x)S_-=(\mu-1)S_-+(d_1+id_2)\partial_x^2S_- -[N|S_-|^2+(N+C^-)|S_+|^2]S_- \tag{A10}$$

with:

$$d_1=\frac{\alpha^2-4a\Delta}{2(\gamma_s+\gamma_i)^2} \quad \text{and} \quad d_2=\frac{a_s-a_i}{2}.$$

[1] S. Longhi, Phys. Rev. A **53**, 4488 (1996); S. Longhi and A. Geraci, *ibid.* **54**, 4581 (1996).

[2] J. Lega, P.K. Jacobsen, J.V. Moloney, and A.C. Newell, Phys. Rev. A **49**, 4201 (1994).

[3] G.-L. Oppo, M. Brambilla, and L.A. Lugiato, Phys. Rev. A **49**, 2028 (1994); M. Tlidi, P. Mandel, and R. Lefever, Phys. Rev. Lett. **81**, 979 (1998); G.J. de Varcacel, K. Staliunas, E. Roldan, and V.J. Sanchez-Morcillo, Phys. Rev. A **54**, 1609 (1996); S. Longhi, J. Mod. Opt. **43**, 1089 (1996).

[4] M.N. Ouarzazi and P.A. Bois, Eur. J. Mech. B/Fluids **13**, 275 (1994); M.N. Ouarzazi, P.A. Bois, and M. Taki, *ibid.* **13**, 423 (1994).

[5] M. Santagiustina, P. Colet, M. San Miguel, and D. Walgraef, Phys. Rev. E **58**, 3843 (1998).

[6] M. Taki, M. San Miguel, and M. Santagiustina, Phys. Rev. E **61**, 2133 (2000).

[7] M. Santagiustina, P. Colet, M. San Miguel, and D. Walgraef, Opt. Lett. **23**, 1167 (1998).

[8] M. Taki, N. Ouarzazi, H. Ward, and P. Glorieux, J. Opt. Soc. Am. B **17**, 997 (2000).

[9] G. Izùs, M. Santagiustina, M. San Miguel, and P. Colet, J. Opt. Soc. Am. B **16**, 1592 (1999).

[10] J.N. Kutz, Th. Erneux, S. Trillo, and M. Healterman, J. Opt. Soc. Am. B **16**, 1936 (1999).

[11] A. Beržanskis, A. Matijošius, A. Piskarskas, V. Smilgevičius, and A. Stabinis, Opt. Commun. **150**, 372 (1998).

[12] H. Ward, M.N. Ouarzazi, M. Taki, and P. Glorieux, Eur. Phys. J. D **3**, 275 (1998).

[13] A. Couairon and J.M. Chomaz, Phys. Rev. Lett. **79**, 2666 (2000); X. Nicolas, A. Mojtabi, and J.K. Platten, Phys. Fluids **9**, 337 (1997).

[14] P. Büchel and M. Lucke, Phys. Rev. E **61**, 3793 (2000).

[15] A. Joulin and M.N. Ouarzazi, C. R. Acad. Sci., Ser. IIb: Mec., Phys., Chim., Astron. **326**, 311 (2000).

[16] T. Nishikawa and N. Uesugi, Opt. Commun. **140**, 277 (1997); J. Appl. Phys. **77**, 4941 (1995); A.V. Smith, W.J. Alford, T.D. Raymond, and M.S. Bowers, J. Opt. Soc. Am. B **12**, 2253 (1995).

[17] M. Vaupel, A. Maitre, and C. Fabre, Phys. Rev. Lett. **83**, 5278 (1999).

[18] P. Huerre and P.A. Monkewitz, Annu. Rev. Fluid Mech. **22**, 473 (1990).

[19] L. Brevdo, ZAMP **42**, 911 (1991).

[20] V.J. Sanchez-Morcillo, E. Roldan, G.J. de Varcacel, and K. Staliunas, Phys. Rev. A **56**, 3237 (1997).

[21] M. Tveitereid and H.W. Müller, Phys. Rev. E **50**, 1219 (1994).